ACADEMIC PRESS

Available online at www.sciencedirect.com

SCIENCE DIRECT®

Journal of Sound and Vibration 265 (2003) 269–287

JOURNAL OF SOUND AND VIBRATION

www.elsevier.com/locate/jsvi

Validation of estimated isotropic viscoelastic material properties and vibration response prediction

M. Dalenbring

Aeronautics Division, FFA, FOI, Swedish Defence Research Agency, P.O. Box 11021, S-161 11 Bromma, Sweden

Received 6 July 2001; accepted 27 June 2002

Abstract

This paper is concerned with finite element (FE) prediction of forced vibrations using a linear viscoelastic constitutive vibration damping modelling technique. A combined numerical and experimental investigation was performed on two bonded aluminium-PMMA (polymethyl methacrylate) plates with different geometry. Three-dimensional FE models were established using experimentally estimated PMMA material properties (elastic and damping) from previously published procedures. The viscoelastic material damping parameters are here validated from the perspective of accurate estimation of constitutive material properties. Vibration responses were predicted from the FE models and measured on the two composite plate structures at a large number of points. Comparisons between the numerical FE simulations and corresponding measured responses show that the estimated material damping properties used as input to the computations are very accurate and may be treated as independent of the geometry and boundary conditions of the plate structures, i.e., as constitutive damping parameters.

1. Introduction

The trend in development of modern transportation systems is to limit the use of prototypes. Instead an increasing focus is put on more and more realistic mathematical models allowing for accurate prediction and optimization of durability and comfort. To correctly predict vibration responses of various types of structures, the availability of accurate models and reliable material data is crucial. Whereas, elastic parameters might be adequately well known, the constitutive modelling of damping is as yet an area of extensive research. One example is the various damping treatments used to reduce vibration problems. Characterization of the materials used in such

E-mail address: dgm@foi.se (M. Dalenbring).

0022-460X/03/$ - see front matter
doi:10.1016/S0022-460X(02)01261-0

treatments is therefore one important preparatory step in the design stage. In this context an important achievement would be the ability to predict vibration responses of arbitrary composite and built-up structural parts comprising high damping materials together with porous and fibrous materials.

Linear, solid, materials may, under isothermal conditions, be characterized by using standard viscoelasticity, which is fully three dimensional, and in the general case, both spatially inhomogeneous and fully anisotropic. See Simo and Hughes [1] and references therein for a thorough exposition of the theory of viscoelasticity and internal variables. For the connection with classical mechanical spring–dashpot models in linear viscoelasticity, see Ref. [2]. For generalizations of the convolution formulation using a continuous relaxation spectrum, see e.g., Ref. [3] and references therein. For connections with fractional derivatives based models/relaxation functions, see Refs. [4,5].

By using the elastic–viscoelastic correspondence principle, cf. Ref. [2], given as a frequency domain augmentation of the standard Hooke's material stiffness matrix, constitutive dynamic material properties (including damping) may be simulated. The material properties are most often extracted indirectly from experimental forced vibration responses given in the form of receptance (vibration displacement response divided by the excitation force in frequency domain) frequency response functions (FRF) and measured on a test structure made from the studied material. These (viscoelastic) properties are material specific, contrary to the engineering structural or modal damping factors traditionally used in vibroacoustic applications, and consequently separated from the elastic (static) material properties, the boundary conditions (imposed by constraints and excitation) and the particular vibrational deformation of the material. For isotropic materials the damping may thus be represented by two complex, frequency-dependent damping functions, cf. Ref. [3]. The chosen parameterization of the viscoelastic material is somewhat optional, cf. Refs. [5,6,7–11], but each candidate parameterization must of course be validated in terms of accuracy in simulation of important viscoelastic phenomena and computational efficiency but also with respect to simplicity and robustness in extraction/estimation of the material damping parameters. The damping function estimation methodology and the particular parameterization used in this paper are described in detail, for homogeneous, isotropic materials, in Refs. [12,13].

In the present paper, vibration response predictions, using finite element (FE) models based on traditional linear viscoelasticity and experimentally determined elasticities and damping functions, are demonstrated for two different composite double-layer aluminium-PMMA (polymethyl methacrylate) plate structures. The predicted responses are compared with vibration responses measured in an experimental investigation of the two physical plate structures.

The objective of the paper is to validate the (three-dimensional) constitutive damping function estimation methodology by showing that experimentally determined material properties, estimated for separate test samples of the material, may then be used for prediction of vibration responses of arbitrarily shaped pieces of the material, including cases when the same pieces are used as parts in built-up, composite structures such as, e.g., the studied double-layer plate structures.

It is assumed that the conditions are isothermal and that the vibrations are small and linear, which is appropriate in most vibroacoustic applications. It is also assumed that each sub-layer of the studied plate structures is isotropic and homogeneous. Finally, if not defined directly in the text, notations used may be found in Appendix A.

2. Linear viscoelastic material models

Consider a viscoelastic solid with N_a discrete relaxation processes, each one characterized by an internal anelastic strain field variable $\varepsilon_n^a(\mathbf{x}, t)$ and a corresponding elastic material stiffness matrix $\mathbf{C}_n^a(\mathbf{x}, t)$, cf. Appendix A. For this model the stress response $\sigma(\mathbf{x}, t)$ is defined by the three-dimensional constitutive relationship, cf. Ref. [1], as

$$\boldsymbol{\sigma}(t) = \mathbf{C}^0\boldsymbol{\varepsilon}(t) - \sum_{n=1}^{N_a} \mathbf{C}_n^a\varepsilon_n^a(t), \tag{1}$$

where the initial (instantaneous) stiffness matrix $\mathbf{C}^0$ is such that the strain energy $\boldsymbol{\varepsilon}\cdot\mathbf{C}^0\boldsymbol{\varepsilon} > 0$ for arbitrary $\boldsymbol{\varepsilon}$. Each internal variable field ε_n^a is governed by the following evolution equation:

$$\dot{\varepsilon}_n^a = \frac{1}{\tau_n}(\boldsymbol{\varepsilon} - \varepsilon_n^a), \quad \lim_{t\to 0}\varepsilon_n^a(t) = 0, \tag{2}$$

where each relaxation time $\tau_n > 0$ and the reference time, initial condition for vanishing anelastic internal strain ε_n^a, is set to $t = 0$.

The convolution form is given by integrating the evolution equation (2) and substitution of the solution into the constitutive equation (1) as

$$\boldsymbol{\sigma}(t) = \mathbf{C}^0\boldsymbol{\varepsilon}(t) - \int_{0^+}^{t} \frac{\mathrm{d}\mathbf{C}(t-u)}{\mathrm{d}u}\boldsymbol{\varepsilon}(u)\,\mathrm{d}u, \tag{3}$$

where the material relaxation function $\mathbf{C}(t)$ is introduced as

$$\mathbf{C}(t) = \mathbf{C}^\infty + \sum_{n=1}^{N_a} \mathbf{C}_n^a \mathrm{e}^{-t/\tau_i}, \tag{4}$$

where $\mathbf{C}^\infty$ is the long-term elastic, fully relaxed, generalized Hooke's law stiffness matrix characterizing all linear solids, such that $\boldsymbol{\varepsilon}\cdot\mathbf{C}^\infty\boldsymbol{\varepsilon} > 0 \ \ \forall\boldsymbol{\varepsilon}$, with components defined in Appendix A. Eq. (4) also yields, by setting $t = 0$, the relation between the long-term elastic or fully relaxed stiffness $\mathbf{C}^\infty$ and the instantaneous stiffness $\mathbf{C}^0 = \mathbf{C}^\infty + \sum_{n=1}^{N_a}\mathbf{C}_n^a$.

Throughout this work a discrete relaxation spectrum is employed. The corresponding Laplace transformed constitutive relation, where $s = \mathrm{i}2\pi f$, $\mathrm{i}^2 = -1$ and f is the current frequency of vibration, yields

$$\tilde{\boldsymbol{\sigma}}(s) = \left[\mathbf{C}^\infty + \sum_{n=1}^{N_a}\frac{s\mathbf{C}_n^a}{s+\beta_n}\right]\tilde{\boldsymbol{\varepsilon}}(s) = [\mathbf{C}^\infty + \mathbf{C}_a(s)]\tilde{\boldsymbol{\varepsilon}}(s), \tag{5}$$

where β_n, $n = 1, 2, 3, \ldots, N_a$, are real positive relaxation frequencies with relaxation times $\tau_n = 1/\beta_n$. For connections with the so-called AHL-theory, see Ref. [7]. Restrictions imposed on the material parameters by thermodynamics and fading memory are discussed in Refs. [1,5,7,14,15–17].

However, for isotropic material symmetry, Hooke's stiffness matrix is simplified and given in terms of the two independent moduli, here expressed in terms of the shear and Lamé modulus $\mathbf{C}^\infty = G\mathbf{C}_G + \lambda\mathbf{C}_\lambda$. The separation chosen here is somewhat optional. In linear viscoelastic applications to nearly incompressible rubber and polymer materials it is natural and more common to use the bulk modulus in order to separate the deformation in terms of the volume

preserving (deviatoric) part and the volume changing (dilatational) part. For large deformations the material properties may be defined in terms of the invariants of the material stiffness tensor.

The constitutive (6×6) frequency-dependent material matrix field, for the case of homogeneous and isotropic materials, is then defined by the corresponding two independent engineering moduli, with the viscoelastic augmentation for isotropic material damping, in Eq. (5), formally given by a viscoelastic correspondence principle, cf. Refs. [2,7], as

$$\mathbf{C}_a(s) = d_G(s) G \mathbf{C}_G + d_\lambda(s) \lambda \mathbf{C}_\lambda \tag{6}$$

in terms of the two constant matrices $\mathbf{C}_G$ and $\mathbf{C}_\lambda$, defined in Appendix A, and G, λ, d_G and d_λ are, respectively, the elastic shear modulus, the elastic Lamé modulus and the two corresponding complex, frequency-dependent, material damping functions. The four parameters G, λ, d_G and d_λ have thus to be specified for each of the two sub-layers of the plates studied, to fully simulate the elastic and dynamical properties of the assembled structures. The real, constant (6×6) matrices $\mathbf{C}_G$ and $\mathbf{C}_\lambda$ are defined in Appendix A. The isotropic damping functions are parameterized as

$$d_G(s) = \sum_{n=1}^{N_a} \frac{s A_G^{(n)}}{(s + \beta_n)}, \tag{7}$$

$$d_\lambda(s) = \sum_{n=1}^{N_a} \frac{s A_\lambda^{(n)}}{(s + \beta_n)}, \tag{8}$$

where the experimental estimation of the real model parameters β_n, $A_G^{(n)}$ and $A_\lambda^{(n)}$ are discussed in Refs. [12,13]. All parameters β_n and $A_G^{(n)}$ are positive and the number, N_a, of discrete damping processes (i.e., the number of terms in Eqs. (7) and (8)), needed to correctly simulate the vibration damping, depends on the material and on the studied range of the vibration frequency f. The parameters $\beta_n = 1/\tau_n$ are relaxation frequencies (given in rad/s) corresponding to a discrete spectrum of positive relaxation times τ_n, according to Eq. (8). The parameters $A_G^{(n)}$ and $A_\lambda^{(n)}$ are referred to as process amplitudes defining the strength of viscoelasticity of the contributing terms in Eqs. (7) and (8).

3. Finite element equations of motion

The standard linear time domain, discrete equations of motion for a structure with material properties are defined by viscoelastic parameters as

$$\mathbf{M}\ddot{\mathbf{X}}(t) + \mathbf{K}_e \mathbf{X}(t) + \int_0^t \mathbf{K}_a(t - \tau)\mathbf{X}(\tau)\, \mathrm{d}\tau = \mathbf{F}(t), \tag{9}$$

where $\mathbf{M}$ and $\mathbf{K}_e$ are the usual mass and stiffness matrices corresponding to the global, degrees of freedom, $\mathbf{X}$, of a traditional displacement formulation, while $\mathbf{F}$ is the corresponding global load vector. Eq. (9) differs from the linear, standard, discrete equations of motion in the way that the traditional damping matrix term, commonly used in vibroacoustic engineering applications, is substituted by a convolution integral, i.e., a memory term corresponding to the viscoelasticity of the material, cf. Refs. [5,18]. Here and in the following, the Laplace transform, with respect to the time variable t, of a field or function is denoted by a tilde above the particular parameter. The

Laplace (frequency) variable is denoted by s and interpreted as the complex number $s = \mathrm{i}\omega$ where ω is the circular frequency in radians per second corresponding to the current frequency of vibration f in Hz. In the complex frequency domain Eq. (9) is equivalent to

$$\left[\mathbf{K}_e + s^2\mathbf{M} + \tilde{\mathbf{K}}_a(s)\right]\tilde{\mathbf{X}}(s) = \tilde{\mathbf{F}}(s). \tag{10}$$

The complex, frequency dependent, viscoelastic contribution $\tilde{\mathbf{K}}_a(s)$ to the global stiffness may be expressed by using standard FE techniques as

$$\tilde{\mathbf{K}}_a(s) = \int_\Omega \mathbf{B}^{\mathrm{T}}\mathbf{C}_a\mathbf{B}\,\mathrm{d}\Omega, \tag{11}$$

where Ω is the volume, in three-dimensional space, occupied by the structure and $\mathbf{B} = \mathbf{B}(\mathbf{x})$ denotes the matrix field relating the approximate, interpolated (small engineering) strains, at spatial points $\mathbf{x}$ in Ω, to the global displacement vector $\mathbf{X}$ of the FE model.

For the two-layer plate structures studied here $\mathbf{C}_a$ is *piecewise continuous* and defined by specifying the four parameters G, λ, $d_G(s)$ and $d_\lambda(s)$ for each of the two sub-layers.

Thus, according to Eq. (11),

$$\tilde{\mathbf{K}}_a(s) = \tilde{\mathbf{K}}_a^{\mathrm{PMMA}}(s) + \tilde{\mathbf{K}}_a^{\mathrm{Al}}(s), \tag{12}$$

where the two contributions are determined by separate integration over the non-overlapping sub-volumes Ω_{Plexi} and Ω_{Al} representing, respectively, the PMMA and the Al.

For comparison, the elastic stiffness matrix $\mathbf{K}_e$ may be expressed as

$$\mathbf{K}_e = \int_\Omega \mathbf{B}^{\mathrm{T}}\mathbf{C}^{\infty}\mathbf{B}\,\mathrm{d}\Omega = \mathbf{K}_e^{\mathrm{PMMA}} + \mathbf{K}_e^{\mathrm{Al}}, \tag{13}$$

where $\mathbf{C}^{\infty}$ is piecewise continuous and, as in Eq. (5), identical to the zero frequency, generalized Hooke's, elastic modulus matrix field of the composite structure.

In the predictions of forced vibration responses presented below the FE equations of motion, Eq. (10), for each of the two test structures were solved using standard direct frequency by frequency matrix inversion. Note also that for zero/vanishing damping the resulting vibration response model, Eq. (10), corresponds to the elastic (undamped) problem.

4. Experimental test cases

4.1. Elastic data, damping properties and FE models used

Material properties were experimentally estimated on separate samples of the PMMA and Al, at approximately the same temperature (room temperature 24°C). The material properties of the PMMA material, given in Tables 1 and 2, are derived using two test samples (plates 1 and 2) and

Table 1
Mean values from measurements of elastic data for the PMMA test plate (average temperature 23°C, humidity 75%)

$E = 3440$ MPa	$\nu = 0.382$	$\rho = 1181$ kg/m^3

the procedures discussed in Ref. [13]. The damping parameters of the PMMA, given in Table 2, are based on vibration measurements in the frequency range 40–500 Hz and should therefore not be considered as representative and complete for simulation of the damping and viscoelasticity of the PMMA outside this frequency range. In accordance with these limitations forced vibrations were predicted only for frequencies within this band. However, it is possible to extend this band by using measured vibrations in an extended frequency interval and adding new dissipation processes by using the methodology described in Ref. [13].

The material damping of the PMMA, Fig. 1, was further assumed to be associated only with $d_G(s)$, i.e., $d_\lambda(s)$ was assumed to be zero. The validity of this simplification has been confirmed, for the studied frequency interval, in a previous paper [12]. Note also that estimated damping data given here is in good agreement with dynamic material data for Perspex given by Read and Dean [19]. The material damping of Al is very small, with a loss factor in the order 10^{-4}, and thus assumed to be negligible in comparison with the damping of the PMMA material.

Elastic (static) material parameters for the Al sample were determined by standard strain-gauge technique and are given in Table 3.

The FE approximation of each test structure comprised a total of 3120 and 1560 isoparametric 20-node (quadratic) volume elements, respectively, for the connected PMMA and Al layers. The FE meshes used are indicated with element boundary lines in Figs. 2 and 3 and were designed to

Table 2
Estimated viscoelastic damping parameters for PMMA

Damping process number (n)	Relaxation frequency ($\beta_n/2\pi$)	Process amplitude ($A_G^{(n)}$)	Process amplitude ($A_\lambda^{(n)}$)
1	1.59×10^{-1}	2.23×10^{-1}	0.0
2	2.26×10^{1}	2.21×10^{-1}	0.0
3	8.21×10^{1}	3.27×10^{-3}	0.0
4	3.14×10^{2}	1.00×10^{-4}	0.0
5	3.84×10^{2}	1.32×10^{-1}	0.0

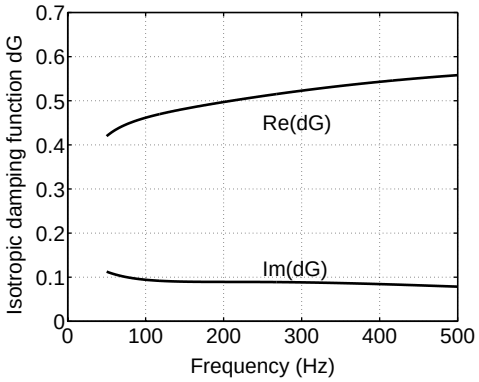

Fig. 1. Isotropic material damping function d_G for PMMA corresponding to elastic data in Table 1 and AHL damping parameters given in Table 2.

Table 3
Mean values from measurements of elastic data for the aluminium test plate (average temperature 25°C)

$E = 73\,000$ MPa	$v = 0.326$	$\rho = 2795\,\mathrm{kg/m^3}$

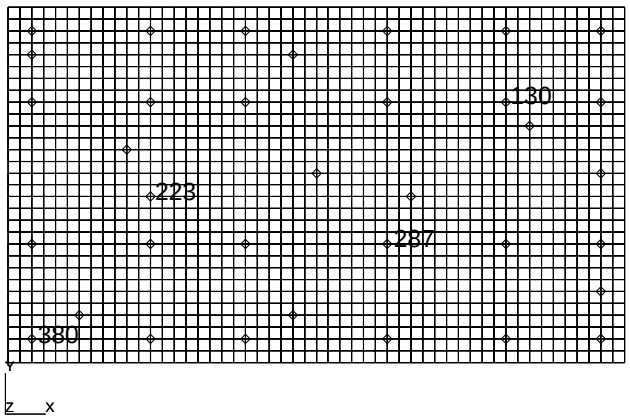

Fig. 2. Measurement points and FE mesh for the layered PMMA-Al plate REC used for validation, using two elements for the PMMA part and one element for the Al part in the thickness direction.

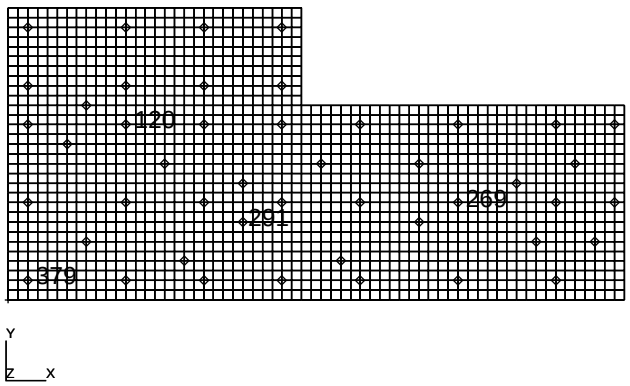

Fig. 3. Measurement points and FE mesh for the layered PMMA-Al plate MOD used for validation, using two elements for the PMMA part and one element for the Al part in the thickness direction.

accurately represent the structures at frequencies in the frequency interval used for the experimental PMMA damping estimation.

4.2. Test set-up, environmental conditions and general measurement specifications

Two different, layered test plates were manufactured from sheets of PMMA and Al. The PMMA sheets used were 7.6 mm thick and the Al sheets were 4.2 mm. One plate was *rectangular*,

$520 \times 300 \times 11.8\,\text{mm}^3$, Fig. 2, and will be referred to as REC. The other plate was *modified*, $630 \times 300 \times 11.8\,\text{mm}^3$ with one edge cut-off $330 \times 100 \times 11.8\,\text{mm}^3$ according to Fig. 3, and will be referred to as MOD. The sheets were first cut to proper geometry and then bonded together using standard epoxy glue. The average thickness of the epoxy layer is 0.06 mm, according to ultrasonic measurements, and is included in the PMMA plate model. This is a reasonable approximation as the material properties of these two material are in the same order, i.e., epoxy have a slightly higher modulus of elasticity and somewhat lower loss factor, cf. Ref. [19], compared to PMMA. This small difference in dynamic material data helps to avoid the epoxy layer from acting as an effective constrained damping layer [20], and the dissipation in the epoxy glue volume will be small relative to the dissipation in the PMMA volume, due to the small thickness of the epoxy layer.

The measured and predicted vibrations are here characterized by frequency response functions (FRFs), in the form of point receptances, $R_{ik} = R_{ik}(\mathbf{x}, \mathbf{x}_e, s)$, defined as quotients between displacement field component spectra $\tilde{u}_i(\mathbf{x}, s)$, at response points $\mathbf{x}$, and corresponding point force component spectra $\tilde{F}_k(\mathbf{x}_e, s)$ at excitation points $\mathbf{x}_e$ on the boundary $\partial\Omega$.

The experimental vibrations (normal velocities) were measured in a laboratory using a laser Doppler vibrometer (LDV) and a standard vibration transfer function measurement technique. The measurements were made at room temperature 24°C in the frequency interval 20–500 Hz with a frequency resolution of 0.5 Hz. A number of FRFs (35 for REC and 46 for MOD) distributed over the outer faces of the PMMA layers were measured (cf. Figs. 2 and 3). During the measurements, each test plate was suspended, with the face oriented vertically, by two long metal strings attached at the nodal lines of the first resonance to minimize suspension damping and simulate stress free boundary conditions, cf. Refs. [19,21]. The non-contacting LDV sensor was chosen in order to minimize the influence of unwanted mechanical disturbances on the test objects.

Excitation was imposed through a sting mounted electrodynamic shaker attached (in reality over a small surface centred) at point 130 on plate REC (cf. Fig. 2) and at point 291 on plate MOD (cf. Fig. 3). The input force was applied to the Al layer, normal to the surface and measured by means of a standard force transducer, attached (glued) to the structure according to the set-up in Ref. [21, Fig. 3.15b].

4.3. Experimental reciprocity

The choice of the LDV sensor for measurement of the vibrations has the advantage of providing high-quality response data. However, even though this is the case, the measured FRFs are affected by the fact that the distributed loading differs from an ideal point force (which was used in the numerical predictions), in an unknown way and to an unknown amount, not counting inaccuracy of the force gauge measuring the applied force resultant. It is common practice, cf. Ref. [21], to study and check, for a specific test set-up, the *lack of reciprocity*, i.e., the *difference between* R_{ik} and R_{ki} for different pairs of points on the structure. The reason for this is that complete reciprocity (symmetry $R_{ik} = R_{ki}$) would be obtained for an idealized point excitation if the response could be measured "at a point" and not, as in reality, as an average over a finite small surface. A vibration FRF measurement may however be of very good quality even though some lack of experimental reciprocity is observed. Here the observed differences $\Delta_{ik} = R_{ik} - R_{ki}$

are used as *an indication* of the level of agreement that may be expected between predictions and measurements as point forces has been used in the numerical simulation of the excitation, provided that we have repeatability in the measurement test set-up.

Lack of reciprocity, observed for a few point pairs on the test plates, is demonstrated in Figs. 4 and 5 for plate REC and Figs. 6 and 7 for plate MOD. Apart from some isolated frequency ranges, an inspection of Figs. 5–7 shows only small differences in the frequency interval 20–500 Hz. For the case in Fig. 4 the lack of reciprocity is more pronounced but not alarming.

To assess the measurement quality, an attempt to evaluate the uncertainty in the measurements was done. Thus, in connection to reciprocity checks of some pairwise "reciprocal" receptances of the two test plates, the mean relative difference in peak amplitudes and peak frequencies in the reciprocal receptances was calculated for all response peaks found in the frequency interval between 50 and 500 Hz. The mean relative difference in peak amplitude, for plate REC, is –0.67%. The relative difference in peak frequency "location" is −0.19%. The corresponding mean relative

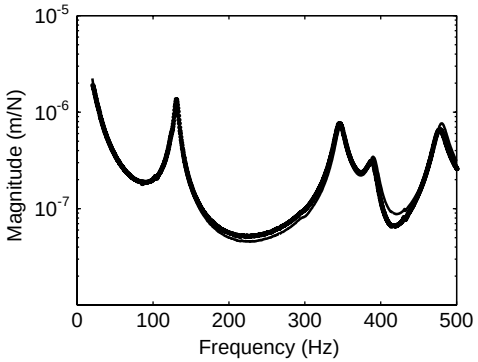

Fig. 4. Reciprocity check for plate REC between measured receptance FRF (response R_{33} in z direction at point 223 and excitation in z direction at point 130; solid line) and measured receptance FRF (response R_{33} in z direction at point 130 and excitation in z direction at point 223; solid-dotted thick line).

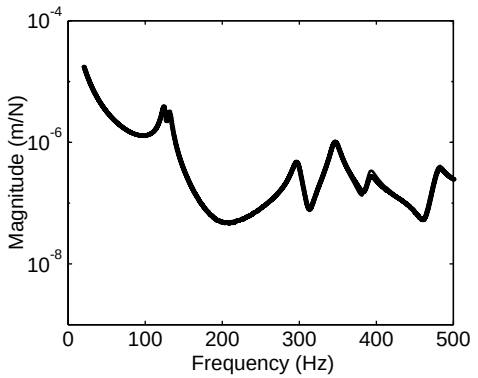

Fig. 5. Reciprocity check for plate REC between measured receptance FRF (response R_{33} in z direction at point 287 and excitation in z direction at point 130; solid line) and measured receptance FRF (response R_{33} in z direction at point 130 and excitation in z direction at point 287; solid-dotted thick line).

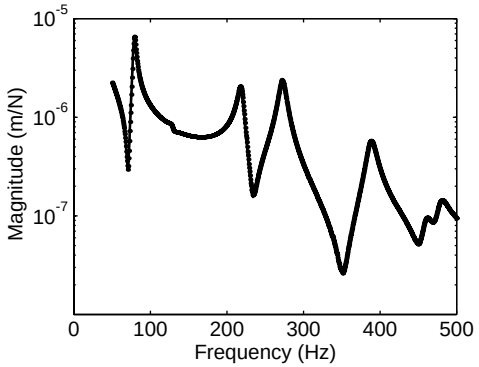

Fig. 6. Reciprocity check for plate MOD between measured receptance FRF (response R_{33} in z direction at point 291 and excitation in z direction at point 269; solid line) and measured receptance FRF (response R_{33} in z direction at point 269 and excitation in z direction at point 291; solid-dotted thick line).

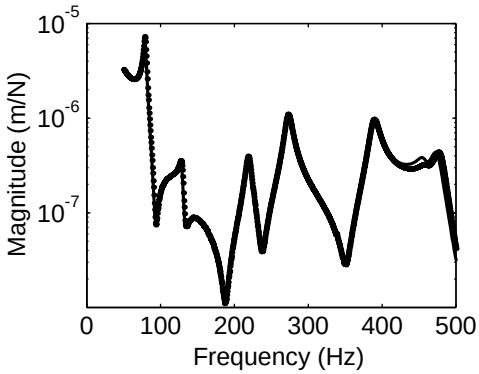

Fig. 7. Reciprocity check for plate MOD between measured receptance FRF (response R_{33} in z direction at point 291 and excitation in z direction at point 120; solid line) and measured receptance FRF (response R_{33} in z direction at point 120 and excitation in z direction at point 291; solid-dotted thick line).

difference in peak amplitude, for plate MOD, is –0.64%. The relative difference in peak frequency location, is 0.06%.

For the validation of the FE predictions, the effect of air damping and damping from the suspension should also be noted. Each of these damping sources may give significant contributions to the total system damping of the suspended plates, cf. Refs. [19,20]. However, for the experimental studied Al-PMMA test plates these loss factors are each estimated to be in the order 10^{-4}. The test structure REC has rather high loss factors ranging from 0.02 to 0.04 in the studied frequency interval, i.e., 200–400 times larger, and the influence of air and suspension damping are thus negligible compared to the damping of PMMA. It is also clear from measured FRFs that the PMMA plays an important role in the vibration response of the composite Al-PMMA structure. This effect may be seen by comparing the first measured resonance frequency 125 Hz of the REC plate, cf. Figs. 4 and 5, and the corresponding frequency of a

homogeneous Al plate with the same dimensions, predicted to 230 Hz. The first eigenfrequency for the Al plate is evidently very different from the REC plate. The vibration response level also depends strongly on the losses in the material. For the REC plate the loss factors η range from 0.02 to 0.04 in the frequency interval 50–500 Hz. These losses are less than the loss factors of PMMA (0.05–0.08) but still large compared to the loss for Al (with η in the order of 10^{-4}), thus indicating that the losses in the REC plate are strongly dominated by PMMA.

4.4. Comparison of predicted and experimental receptances

Receptances R_{ik} were calculated for all measurement points on the test structures, in the frequency interval 100–500 Hz for plate REC and 50–500 Hz for plate MOD, with a frequency resolution of 2.5 Hz.

To evaluate the large amount of data involved, some statistical analysis was performed. For each peak in amplitude of the simulated receptance the difference, between predicted and measured response, in amplitude level and in frequency of the peak, were calculated. Following this, the mean value of the differences in peak amplitude and peak frequency were then calculated.

4.4.1. Validation on plate REC

A selection of the results of the direct FE calculations for plate REC are shown together with the measured receptances in Figs. 8–11. From visual inspection it may be concluded that, the agreement between simulated and measured vibration spectra is in general very good. The relative mean of the peak amplitude difference, based on all five response peaks, for plate REC was found to be 1.95% while the relative mean difference in the frequency of the peaks was −0.66%. The relative mean of the peak amplitudes for each of the five response peaks are shown in Fig. 12a and listed in Table 4 together with the relative mean difference in the frequencies, Fig. 12b. These values should be viewed in relation to experimental reciprocity discussed in Section 4.3, i.e., a mean relative difference in amplitude of −0.68% and a mean relative difference in peak frequency of −0.19%.

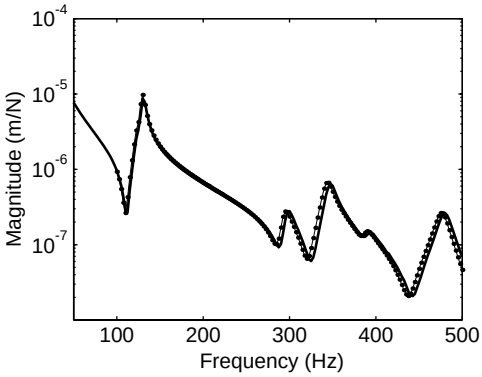

Fig. 8. Measured (solid line) point receptance FRF for plate REC (response R_{33} in z direction at point 130 and excitation in z direction at point 130) and direct FE calculation (solid-dotted line).

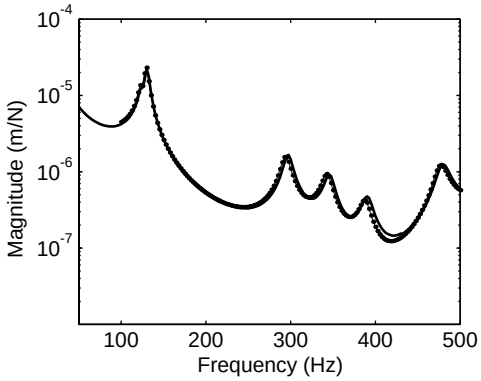

Fig. 9. Typical measured (solid line) transfer receptance FRF for plate REC (response R_{33} in z direction at point 380 and excitation in z direction at point 130) and direct FE calculation (solid-dotted line).

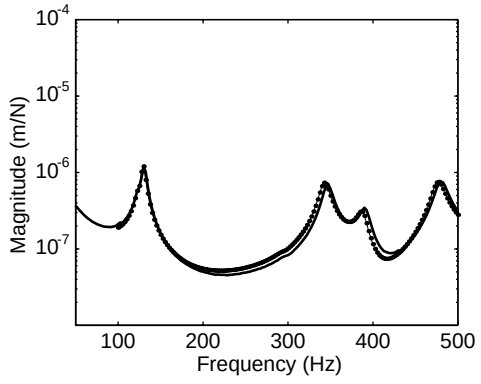

Fig. 10. Typical measured (solid line) transfer receptance FRF for plate REC (response R_{33} in z direction at point 223 and excitation in z direction at point 130) and direct FE calculation (solid-dotted line).

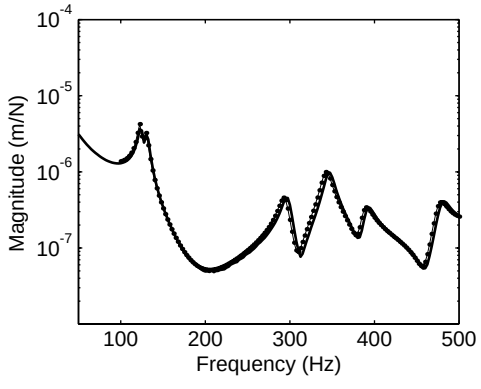

Fig. 11. Typical measured (solid line) transfer receptance FRF for plate REC (response R_{33} in z direction at point 287 and excitation in z direction at point 130) and direct FE calculation (solid-dotted line).

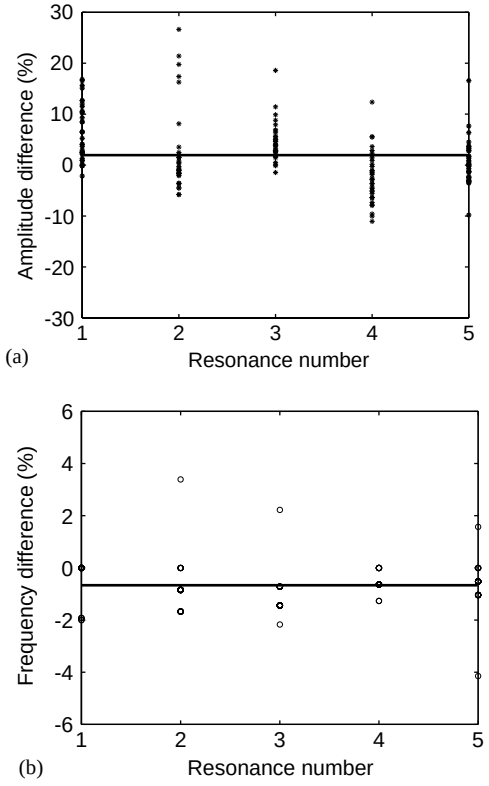

Fig. 12. (a) Peak amplitude level and (b) peak frequency difference between measured and AHL simulated receptance on plate REC. Evaluated for all 35 receptance FRFs at five response peaks. (* = amplitude difference, o = frequency difference).

Table 4
Mean differences for plate REC at five resonance peaks

Peak number	Peak frequency in exp FRF (Hz)	Mean value amplitude (%)	Mean value frequency (%)
1	130.0	6.37	−0.28
2	297.5	2.15	−0.79
3	347.5	3.08	−1.07
4	392.5	−2.40	−0.53
5	480.0	0.53	−0.65

4.4.2. *Validation on plate MOD*

A selection of the results of the direct FE calculations for plate MOD are shown together with the measured receptances in Figs. 13–16. Also for this test case, visual inspection leads to the conclusion that the agreement between simulated and measured vibration spectra is in general satisfying. The relative mean of the peak amplitude difference, based on all six response peaks, for plate MOD was found to –0.92% while the relative mean difference in the frequency of the peaks was –0.53%. The relative mean of the peak amplitudes for each of the six response peaks are shown in Fig. 17a and listed in Table 5 together with the relative mean difference in the

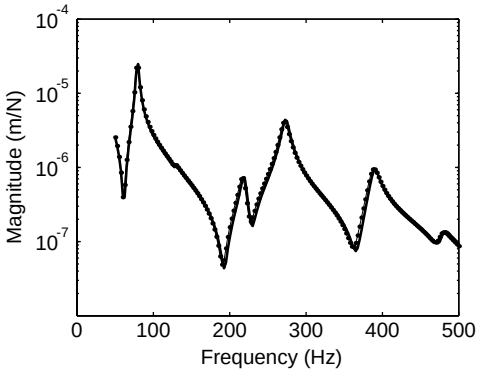

Fig. 13. Measured (solid line) point receptance FRF for plate MOD (response R_{33} in z direction at point 291 and excitation in z direction at point 291) and direct FE calculation (solid-dotted line).

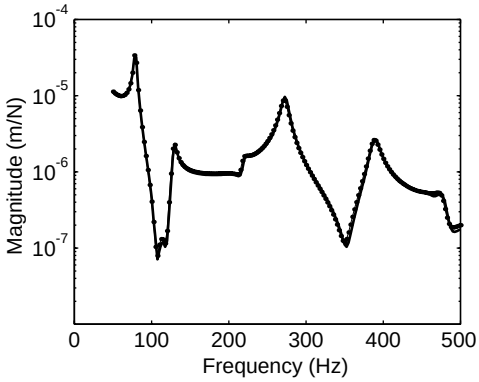

Fig. 14. Typical measured (solid line) transfer receptance FRF for plate MOD (response R_{33} in z direction at point 379 and excitation in z direction at point 291) and direct FE calculation (solid-dotted line).

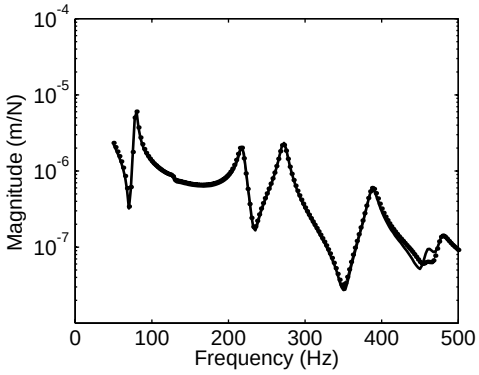

Fig. 15. Typical measured (solid line) transfer receptance FRF for plate MOD (response R_{33} in z direction at point 269 and excitation in z direction at point 291) and direct FE calculation (solid-dotted line).

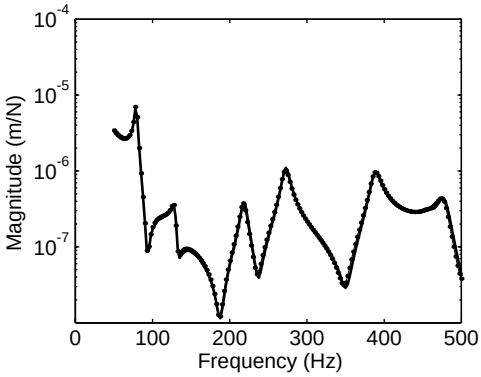

Fig. 16. Typical measured (solid line) transfer receptance FRF for plate MOD (response R_{33} in z direction at point 120 and excitation in z direction at point 291) and direct FE calculation (solid-dotted line).

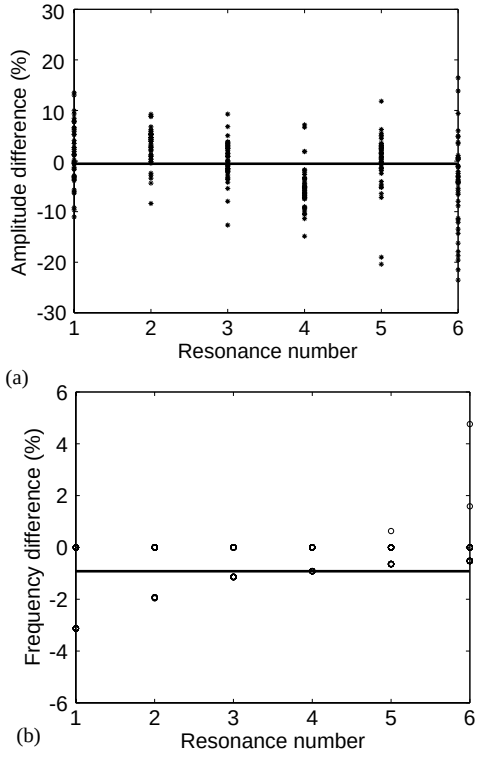

Fig. 17. (a) Amplitude level and (b) peak frequency difference between measured and AHL simulated receptance on plate MOD. Evaluated for all 46 receptance FRFs at six response peaks. (* = amplitude difference, o = frequency difference).

frequencies, Fig. 17b. Comparing these to the experimental reciprocity discussed in Section 4.3, i.e., mean relative difference in amplitude –0.64% and mean relative difference in peak frequency 0.06%, reveal that the discrepancy between the simulations and the measurements is of the same order as the observed lack of experimental reciprocity.

Table 5
Mean differences for plate MOD at six resonance peaks

Peak number	Peak frequency in exp. FRF (Hz)	Mean value amplitude (%)	Mean value frequency (%)
1	77.5	1.27	−1.63
2	130.0	2.98	−0.29
3	220.0	0.11	−0.55
4	272.5	−5.44	−0.30
5	387.5	−0.09	−0.22
6	475.0	−4.35	−0.17

4.4.3. Discussion of results from comparison

Evidently, the two FE models, based on isotropic material damping functions, provide accurate simulations of the measured vibration responses in the studied frequency intervals.

The damping parameters used in the predictions were estimated from frequency response data collected in tests on separate sheets of PMMA while here, in the response measurements, PMMA was glued to an Al sheet. Thus, it may be argued that the estimated constitutive damping parameters are accurate and independent of boundary conditions.

Furthermore, the PMMA sheets used to provide estimates of the damping parameters were rectangular while plate MOD is an L-shaped layered plate. Thus, the estimated damping model used is valid independent of geometry and size variations used here.

For plate REC, it is illustrative to study Fig. 4 and compare with Fig. 10. The slight lack of experimental reciprocity (mainly an amplitude difference) found in the anti-resonances between points 130 and 223, Fig. 4, is visible as a corresponding amplitude difference between simulated and measured frequency response function between excitation at point 130 and response at point 223, Fig. 10.

The situation is slightly different when points 130 and 287 are compared. The lack of experimental reciprocity, Fig. 5, is small up to about 380 Hz. Simulated and measured frequency response curves, Fig. 11, agree in amplitude while there is a clear frequency shift downwards in the simulation results throughout the whole studied frequency range.

For plate MOD, observed experimental reciprocity is in general excellent, see Figs. 6 and 7, with the only exception of importance occurring at around 450 Hz for points 120 and 291. The agreement between simulated and measured frequency response is correspondingly very good, Figs. 13–16, with one exception. For excitation applied at point 291 and response in point 269, Fig. 15, the simulated response does not exhibit the resonance peak at 460 Hz, despite excellent measurement reciprocity for these two points, Fig. 6.

Thus, in general the simulated responses agree with the measured when the observed experimental reciprocity is satisfactory. For plate REC, the lack of experimental reciprocity and also the agreement between simulation and measurement is worse than for plate MOD. The main reason for this is that the excitation applied for plate REC is further away from the mass centre of the plate than for plate MOD. This induces a rigid body rotational component of plate REC, affecting both reciprocity and FRFs, which is seen as a systematic shift of the peak frequencies for excitation in point 130 point.

Obviously, there are a multitude of sources of discrepancies between the simulation and the measurement. Examples of these are: the simulation assumes a point force while in the measurement a distributed load (the attachment of the dynamic shaker) is applied; here only the normal component of the excitation is measured (by the force transducer) while neglecting contribution from unmeasured lateral and moment excitation; the simulation model assumes a uniform thickness of the PMMA sheet while in the test set-up a variation in thickness of 10% is observed; the simulation model assumes a perfect bonding with a negligible thickness of the glueing layer between the PMMA and the Al sheets while the real bonding layer has a finite and possibly varying thickness. Of these the first two points, i.e., the effects of the applied excitation has been discussed by Maia et al. [21] and Olbrechts et al. [22].

5. Summary

A vibration simulation, for two different PMMA-Al plates, is established, based on experimentally determined elasticities and material damping functions, and direct FE calculations. For the two materials the relevant parameters, i.e., mass density, elastic data and isotropic material damping parameters, have been estimated separately. The first question to be answered during this investigation has been concerned with the ability to estimated isotropic elasticities and material damping functions, to predict vibration responses from knowledge about the separate parts, in a built-up structure. Secondly, strengthen the fact that the material parameters are indeed, material properties, rather than system properties of the test used to determine them. This is demonstrated by comparisons between measured vibration responses and numerical predictions using direct FE calculations. The simulated results show excellent agreement with the measurements in the whole frequency interval 50–500 Hz, respectively. It is further argued through experimental reciprocity considerations, that the contribution to differences between measurements and simulations mainly come from uncertainties in the vibration measurements.

Acknowledgements

This work was performed under contract from the Swedish Defence Material Administration (Contract No. 50562-LB78548). The funding provided is gratefully acknowledged. Thanks also to Krister Dovstam, Peter Göransson, Niklas Sehlstedt and Adam Zdunek for valuable comments and help during the preparation of the manuscript.

Appendix A. Definitions

The Cartesian matrix representations $\mathbf{u}, \boldsymbol{\sigma}$ and $\boldsymbol{\varepsilon}$ of the displacement field and the symmetric stress and (infinitesimal) strain tensor fields, respectively, are defined as:

$$\mathbf{u} = \mathbf{u}(\mathbf{x}, t) = \begin{bmatrix} u_1 & u_2 & u_3 \end{bmatrix}^{\mathrm{T}}, \tag{A.1}$$

$$\boldsymbol{\sigma} = \boldsymbol{\sigma}(\mathbf{x}, t) = \begin{bmatrix} \sigma_{11} & \sigma_{22} & \sigma_{33} & \sigma_{12} & \sigma_{23} & \sigma_{31} \end{bmatrix}^{\mathrm{T}}, \tag{A.2}$$

$$\boldsymbol{\varepsilon} = \boldsymbol{\varepsilon}(\mathbf{x}, t) = \begin{bmatrix} \varepsilon_{11} & \varepsilon_{22} & \varepsilon_{33} & 2\varepsilon_{12} & 2\varepsilon_{23} & 2\varepsilon_{31} \end{bmatrix}^{\mathrm{T}}, \tag{A.3}$$

$$\varepsilon_{ik} = \frac{1}{2}\left\{\frac{\partial u_i}{\partial x_k} + \frac{\partial u_k}{\partial x_i}\right\}, \tag{A.4}$$

where u_i, σ_{ik} and ε_{ik} are Cartesian vector and tensor components. The elastic generalized Hooke's law is expressed as

$$\mathbf{C}^{\infty} = G\mathbf{C}_G + \lambda\mathbf{C}_{\lambda}, \tag{A.5}$$

where the only *non-zero elements* of the real, constant (6×6)-matrices $\mathbf{C}_{\lambda}$ and $\mathbf{C}_G$ are:

$$(\mathbf{C}_{\lambda})_{ik} = 1, \quad i, k \leqslant 3, \tag{A.6}$$

$$(\mathbf{C}_G)_{ii} = 2, \quad 1 \leqslant i \leqslant 3, \quad (\mathbf{C}_G)_{ii} = 1, \quad 4 \leqslant i \leqslant 6. \tag{A.7}$$

The Lame moduli G (shear modulus) and λ, expressed in Young's modulus E and the Poisson ratio v $(-1 < v < 0.5)$, are

$$G = \frac{E}{2(1+v)}, \tag{A.8}$$

$$\lambda = \frac{2vG}{(1-2v)}. \tag{A.9}$$

References

[1] J.C. Simo, T.J.R. Hughes, Computational Inelasticity, Interdisciplinary Applied Mathematics, Springer, New York, 1998 ISBN 0-387-97520-9.
[2] W. Flügge, Viscoelasticity, Blaisdell Publishing Company, New York, 1967.
[3] D.F. Golla, P.C. Hughes, Dynamics of viscoelastic structures—a time domain, finite element formulation, Journal of Applied Mechanics 52 (1985) 897–906.
[4] P.J. Torvik, R.L. Bagley, Fractional calculus—a different approach to the analysis of viscoelastically damped structures, American Institute of Aeronautics and Astronautics Journal 21 (1984) 741–748.
[5] M. Enelund, Division of Solid Mechanics, Fractional Calculus and Linear Viscoelaticity, Ph.D. Thesis, Chalmers University of Technology, Göteborg, Sweden, 1996.
[6] L. Gaul, The influence of damping on waves and vibrations, Mechanical Systems and Signal Processing 13 (1) (1999) 1–30.
[7] K. Dovstam, Augmented Hooke's law in frequency domain. A three dimensional material damping formulation, International Journal of Solids Structures 32 (1995) 2835–2852.
[8] K. Dovstam, Research, Augmented Hooke's law based on alternative stress relaxation models, Journal of Computational Mechanics 26 (2000) 90–103.
[9] K. Dovstam, Receptance model based on isotropic damping functions and elastic displacement modes, International Journal of Solids Structures 34 (1997) 2733–2754.
[10] K. Dovstam, Department of Solid Mechanics, Royal Institute of Technology (KTH), 1998 On Material Damping Modelling and Modal Analysis in Structural Dynamics, Ph.D. Thesis, Stockholm, Sweden, 1998.
[11] K. Dovstam, Simulation of damped vibrations based on augmented Hooke's law and elastic modes of vibration, International Journal of Solids Structures 37 (2000) 5413–5544.

[12] K. Dovstam, M. Dalenbring, Damping function estimation based on modal receptance models and neural nets, Research Journal Computational Mechanics 19 (1997) 271–286.
[13] M. Dalenbring, Damping Function Estimation Based on Measured Vibration Frequency Responses and Finite-Element Displacement Modes, Mechanical Systems and Signal Processing 13 (4) (1999) 547–569.
[14] M.A. Biot, Variational principles and irreversible thermodynamics with application to viscoelasticity, Physical Review 97 (1955) 1463–1469.
[15] M.A. Biot, Thermoelasticity and irreversible thermodynamics, Journal of Applied Physics 27 (3) (1956) 240–253.
[16] G.A. Lesieutre, E. Bianchini, Time domain modeling of linear viscoelasticity using anelastic displacement fields, Transactions of the American Society of Mechanical Engineers 117 (1995) 424–430.
[17] R.M. Christensen, Mechanics of Composite Materials, Wiley, New York, 1979 ISBN 0-89464-501-3.
[18] K. Dovstam, Real modes of vibration and hybrid modal analysis, Research Journal of Computational Mechanics 21 (1998) 493–511.
[19] B.E. Read, G.D. Dean, The Determination of Dynamic Properties of Polymers and Composites, Wiley, New York, 1978 ISBN 0-470-26543-4.
[20] L. Cremer, M. Heckl, Structure-Borne Sound, 2nd Edition, Springer, New York, 1987 ISBN 0-387-18241-1.
[21] N.M.M. Maia, J.M.M. Silva, J. He, N.A.J. Lieven, R.M. Lin, G.W. Skingle, W.-M. To, A.P.V. Urgueria, Theoretical and Experimental Modal Analysis, Research Studies Press Ltd., Baldock, Hertfordshire, England, 1997 ISBN 0-86380-208-7.
[22] T. Olbrechts, D. Vandepitte, P. Sas, W. Heylen, Influence of excitation system on the dynamic behaviour of test structures, Proceedings of the ISMA, Vol. 21, Leuven, Belgium, 1996, pp. 881–891.